Experimental Study on the Electrical Conductivity of Pyroxene Andesite at High Temperature and High Pressure

KeShi Hui,[1,2] LiDong Dai,[1] HePing Li,[1] HaiYing Hu,[1,3] JianJun Jiang,[1,2] WenQing Sun,[1,2] and Hui Zhang[1]

Abstract—The electrical conductivity of pyroxene andesite was in situ measured under conditions of 1.0–2.0 GPa and 673–1073 K using a YJ-3000t multi-anvil press and Solartron-1260 Impedance/Gain-phase analyzer. Experimental results indicate that the electrical conductivities of pyroxene andesite increase with increasing temperature, and the electrical conductivities decrease with the rise of pressure, and the relationship between electrical conductivity (σ) and temperature (T) conforms to an Arrhenius relation within a given pressure and temperature range. When temperature rises up to 873–923 K, the electrical conductivities of pyroxene andesite abruptly increase, and the activation enthalpy increases at this range, which demonstrates that pyroxene andesite starts to dehydrate. By the virtue of the activation enthalpy (0.35–0.42 eV) and the activation volume (-6.75 ± 1.67 cm^3/mole) which characterizes the electrical properties of sample after dehydration, we consider that the conduction mechanism is the small polaron conduction before and after dehydration, and that the rise of carrier concentration is the most important reason of increased electrical conductivity.

Key words: Electrical conductivity, Pyroxene andesite, Dehydration, Conduction mechanism, High pressure.

1. Introduction

Alongside developments in measurement technology and experimental equipment, geologists have obtained more and more valuable data regarding electrical properties which help to interpret the chemical composition and distribution of the Earth's interior rocks. Despite numerous notable achievements in this area, researchers continue to dispute the origin and composition of the high conductivity zone ($\sigma > 10^{-2}$ S/m) in the crust (Christensen and Mooney 1995; Vanyan and Gliko 1999; Shinoda et al. 2002; Nover 2005; Huang et al. 2005a, b, 2012; Dai and Karato 2009, 2014a). By means of experimental simulation and calculation at high temperature and pressure, researchers consider that due to plate tectonics and metamorphism, the dehydration of water-bearing rocks producing free water is a rational reason for the high conductivity zone. Therefore, studies on electrical properties have considerable scientific significance in rocks which contain hydrous minerals (constitution water or crystal water).

Andesite, containing plagioclase, amphibole, pyroxene, quartz and biotite, is widely distributed in the active plate convergence margin (active continental margin, orogenic belt and island arc) (Ferri et al. 2013; Hui et al. 2015). A large amount of data on the electrical conductivity of andesite have been achieved until now. Waff and Weill (1975) measured the electrical conductivities of andesite with different components of Na_2O (4.96–7.83 wt%) and FeO (4.99–13.7 wt%) under room pressure and different oxygen partial pressures of CO_2 and H_2, and suggested that the electrical conductivities of the sample increased in accordance with increasing alkali ion content, and were not dependent on oxygen fugacity or iron content. Later, by integrating the electrical conductivity data of tholeiite, Tyburczy and Waff (1983) concluded that the electrical conductivities of andesite melts increase with the rise of pressure, and that minimum melt faction of 5–10 % can be used to explain the anomalously high electrical conductivity of the upper mantle in typical andesite regions.

[1] Key Laboratory of High-Temperature and High-Pressure Study of the Earth's Interior, Institute of Geochemistry, Chinese Academy of Sciences, Guiyang, 550002, China. E-mail: dailidong_2014@hotmail.com
[2] University of Chinese Academy of Sciences, Beijing 100049, China.
[3] Key Laboratory of Earth and Planetary Physics, Institute of Geology and Geophysics, Chinese Academy of Sciences, Beijing 100029, China.

Recently, Laumonier et al. (2015) measured the electrical conductivity of deictic melts with H_2O content up to 12 wt% at pressures of 0.15–3.0 GPa and temperatures of 673–1573 K, and demonstrated that the electrical conductivity of dacitic melts increased with increasing water content. By means of T-P-H_2O model, crustal and mantle wedge conductive bodies have been interpreted by the presence of silica-rich, hydrous, partially crystallized magma. However, previous researches were primarily focused on the effects of partial melting, rather than considering the effects of dehydration on the electrical conductivity for andesite.

In this study, the electrical conductivity of pyroxene andesite was measured at pressures of 1.0–2.0 GPa, temperatures of 673–1073 K and frequency range from 10^{-1} to 4×10^6 Hz. The characteristic parameters of the electrical conductivity of pyroxene andesite were acquired, including the activation enthalpy, the activation energy and the activation volume. According to these parameters, the effects of temperature, pressure and dehydration on the electrical conductivity of the sample have been discussed, as well as the conduction mechanism before and after dehydration.

2. Experiment

2.1. Sample Preparation

The experimental andesite was chosen from Lvliang, Shanxi Province, China. The sample was gray–green, fresh, non-oxidized, and contained fine-grain pyroxene (~ 15 %), amphibole (~ 25 %) and plagioclase (~ 60 %) phenocrysts (Fig. 1a). To explore the chemical composition and mineralogical proportion, the sample was determined with the X-ray fluorescence spectrometer (XRF) and electron microprobe analysis (EPMA) at the State Key Laboratory of Ore Deposit Geochemistry, Institute of Geochemistry, Chinese Academy of Sciences, Guiyang, China and a back-scattered electron image was also achieved. Results are showed in Table 1 and Fig. 1b. Total alkali and silica (TAS) classification was used to confirm the precise name of the sample as pyroxene andesite (Fig. 2).
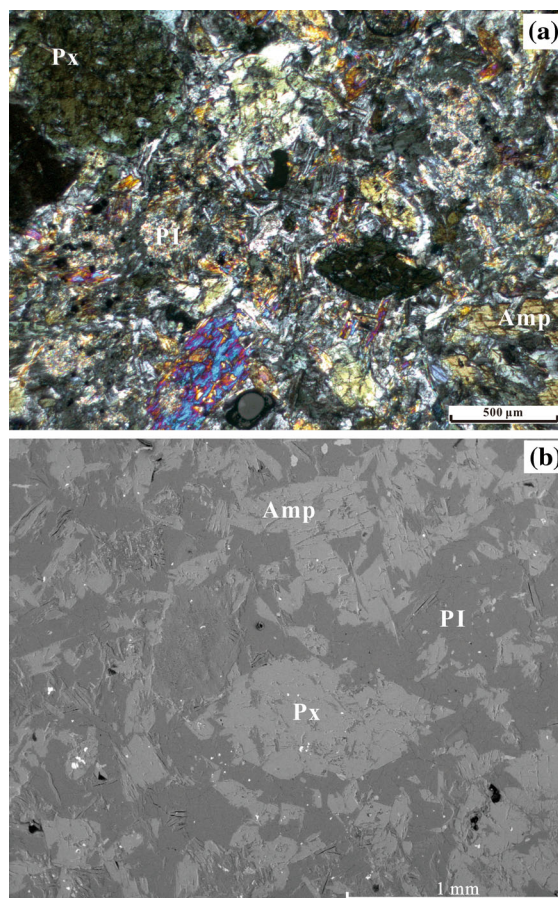

Figure 1
Abbreviations in the figure represent *Px* pyroxene, *Amp* amphibole and *PI* plagioclase, respectively. **a** The photomicrograph of pyroxene andesite before experiment. **b** The back-scattered electron image from the analysis of pyroxene andesite before experiment

Before experiment, the pyroxene andesite was cut into cylinders each 6 mm in diameter and 6 mm in height. The cylindrical samples were then cleaned in an ultrasonic cleaning device using the deionized water, acetone and ethanol in turn. To avoid the influence of absorbed water on the conductivity measurements, all of the cylindrical samples were baked at 323 K for 12 h in an oven.

2.2. Experiment

Electrical conductivity measurements were carried out in the YJ-3000t multi-anvil apparatus and Solartron-1260 Impedance/Gain-phase analyzer in the Key Laboratory of High-Temperature and High-Pressure Study

Table 1

Chemical composition of whole rock analysis and main minerals of pyroxene andesite

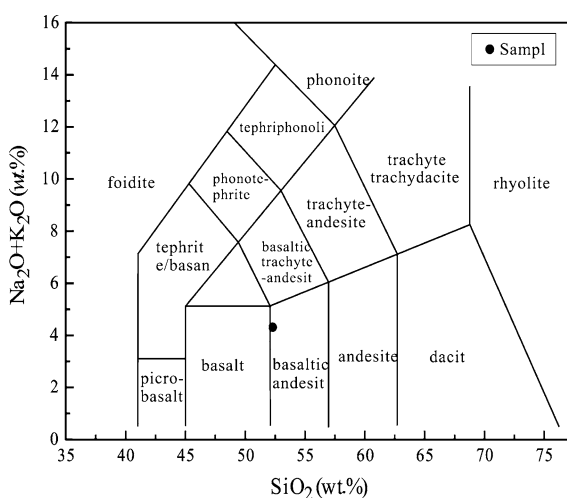| Oxides	XRF for whole rock (wt%)	EPMA for plagioclase (wt%)	EPMA for pyroxene (wt%)	EPMA for amphibole (wt%)
SiO_2	52.16	67.67	44.59	45.06
Al_2O_3	11.79	20.20	11.39	10.63
MgO	12.56	0	12.43	16.58
CaO	5.55	0.31	11.82	11.53
Na_2O	4.04	11.70	1.48	2.05
K_2O	0.28	0.08	0.62	0.59
FeO	8.02	0.01	15.89	9.42
TiO_2	0.52	0	1.18	1.03
Cr_2O_3	–	0.01	0.26	0.15
MnO_2	0.10	0	0.21	0.13
P_2O_5	0.15	–	–	–
L.O.I	4.65	–	–	–
Total	99.82	99.98	99.87	97.17

Figure 2
TAS (total alkali and silica) classification of igneous rock

of the Earth's Interior, Institute of Geochemistry, Chinese Academy of Sciences. A detailed description of the equipment (Fig. 3), and the experimental process used in this work can be found in the previous studies by Dai et al. (2013) and Hu et al. (2015). As shown in Fig. 3, the cubic pyrophyllite ($32.5 \times 32.5 \times 32.5$ mm^3) was used as the pressure medium, and the heater was composed of three-layer stainless steel sheets (total thickness: 0.5 mm) in the shape of a tube. The alumina and magnesia sleeve were adopted to ensure that the sample was in a relatively insulated environment, and the 0.025-mm-thickness nickel foil which shield the external electromagnetic and spurious signal interference was placed in the middle of alumina and magnesia sleeve. The electrodes on both sides of sample were composed of two nickel disks (thickness: 0.5 mm and diameter: 6 mm). As shown in previous studies, to prevent the influence of dehydration on the impedance spectroscopy measurement, all the experimental parts, including the pyrophyllite, the alumina and magnesia sleeve were heated at 1173 K for 12 h in a muffle furnace. Temperature was monitored using a NiCr-NiAl thermocouple at deviation of ± 10 K. Besides, the equipment described above was similar to Dai et al. (2015, 2016). The oxygen fugacity was well controlled by the metallic electrodes and nickel foil.

During the experiment, pressure was raised at a rate of 1.0 GPa/h until it reaches the designed pressure, and then temperature was increased at a rate of 100 K/h. Once the temperature reached each preset value, a Solartron-1260 Impedance/Gain-phase analyzer was used to collect the impedance semicircular arc with the measuring signal voltage of 1 V and frequency of 10^{-1}–4×10^6 Hz which is characterized by the electrical properties of the sample. To ensure the reliability of the experimental results, the impedance spectra of samples were measured several times at each temperature until two similar impedance semicircular arcs were collected.

3. Experimental Results

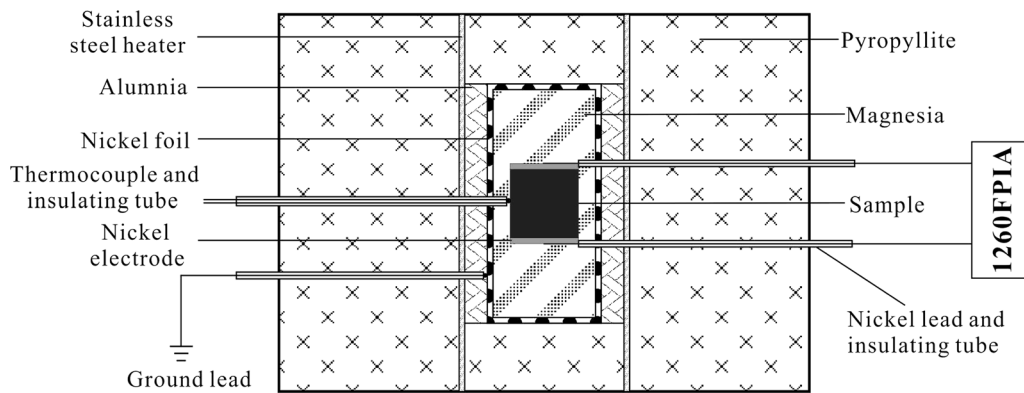Nyquist and Bode plots of the complex impedance of pyroxene andesite under conditions of 1.0 GPa,

Figure 3
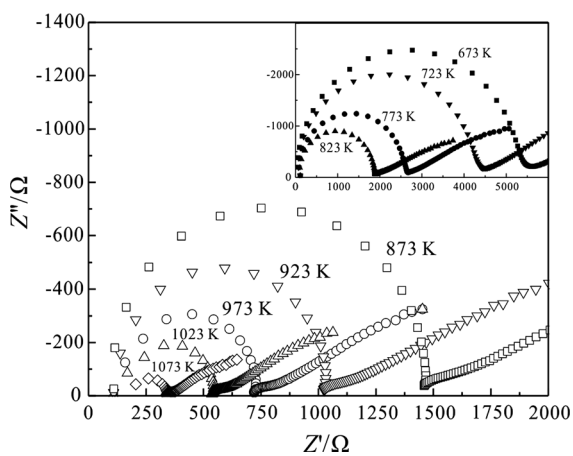Experimental setup of electrical conductivity measurements

Figure 4
Nyquist plot of the complex impedance of pyroxene andesite under conditions of 1.0 GPa and 673–1073 K. Z' and Z'' is real part and imaginary part, respectively

Figure 5
Bode plot of pyroxene andesite under conditions of 1.0 GPa and 673–1073 K. |Z|, θ and f are modulus, phase angle and frequency

673–1073 K and 10^{-1}–4×10^6 Hz are shown in Figs. 4 and 5. As shown in Fig. 4, the diameter of impedance arcs and the impedance values decrease rapidly as temperature increases. Each impedance arc contains two parts, each of which has a different characteristic relaxation time: one semicircular arc at high frequencies (10^2–4×10^6 Hz) represents the conduction process of the grain interior, and the other part which appears at lower frequencies (10^{-1}–10^2 Hz) reflects the typical characteristic of diffusion process at the sample–electrode interface (Roberts and Tyburczy 1991). To this effect, only the high-frequency arc was used to determine the electrical conductivity of the sample. From the Bode plot (Fig. 5), it is shown that the impedance modulus
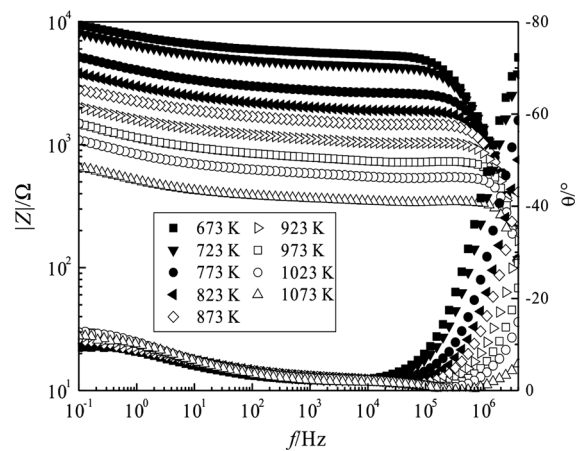
increases rapidly, and the absolute value of phase angle tends to zero from high to low frequency. According to the impedance spectroscopy theory (Nover et al. 1992; Huebner and Dillenburg 1995), the real part (Z'), the imaginary part (Z''), modulus (|Z|), and phase angle (θ) are described as: $Z' = |Z| \cos \theta$ and $Z'' = |Z| \sin \theta$.

The grain interior resistance of pyroxene andesite was fitted using the series connection of RC. The electrical conductivity of sample is in accordance with the following expression:

$$\sigma = L/SR \tag{1}$$

where L is the sample length (m), S is the cross-sectional area of the electrode (m^2), and R is the resistance of the sample (Ω).

At the pressures of 1.0–2.0 GPa and temperatures of 673–1073 K, the relationship between electrical conductivity of quartz andesite (σ) and reciprocal temperature ($1/T$) was fitted using the Arrhenius linear relation:

$$\sigma = \sigma_0 \exp(-\Delta H/kT) \qquad (2)$$

where σ_0 is the pre-exponential factor (S/m), ΔH is the activation enthalpy (eV), k is the Boltzmann constant, and T is the absolute temperature (K). The relationship among activation energy ΔU (eV), pressure P (GPa), and activation volume ΔV (cm^3/mole) is expressed as follows:

$$\Delta H = \Delta U + P \times \Delta V \qquad (3)$$

As shown in Fig. 6, conductivity data from first heating cycle were apparently lower than those from subsequent heating and cooling cycles, and increased rapidly once temperature reached 873 K. The ratio of electrical conductivity dependence on temperature under 1.0–2.0 GPa is shown in Fig. 7. Table 2 shows the activation enthalpy, the activation volume and the pre-exponential factor which were calculated using Eq. (2).

4. Discussions

In this work, the electrical conductivity of pyroxene andesite was in situ measured under conditions of 1.0–2.0 GPa and 673–1073 K. The electrical conductivity of sample decreases with the rise of pressure, and the activation enthalpy decreases accordingly. In addition, the activation energy (ΔU), the activation volume (ΔV) and the pre-exponential factor (Log σ_0) after dehydration are 0.48 ± 0.04 eV, −6.75 ± 1.67 cm^3/mole and 1.00–1.31 S/m, respectively.

Previous studies have investigated the electrical conductivity of andesite dependence on pressure; however, all of these were concentrated on the effects of partially molten andesite (Fig. 8). The electrical conductivities of pyroxene andesite in this study are consistent with that of dacitic melts with 7.1 wt% water, and higher than that of anhydrous dacitic melts measured by Laumonier et al. (2015). The electrical conductivity values also fall within the same interval as results obtained by Waff and Weill (1975) and Tyburczy and Waff (1983). While the activation
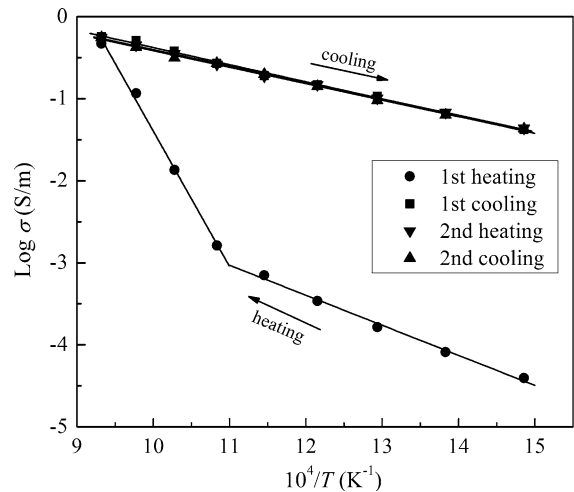

Figure 6
The relation of electrical conductivity and reciprocal temperature of pyroxene andesite under conditions of 1.0 GPa and 673–1073 K
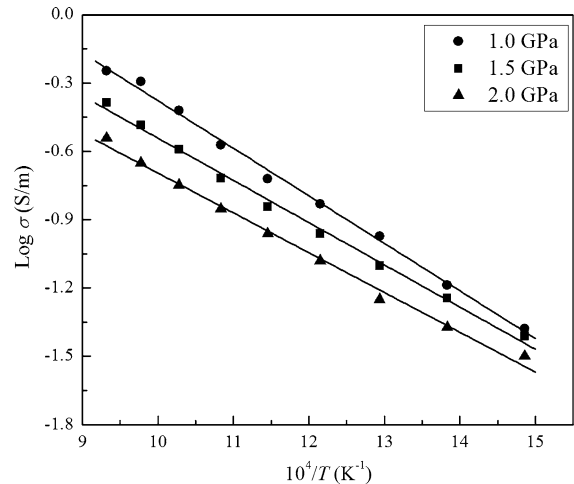

Figure 7
The relation of electrical conductivity and reciprocal temperature of pyroxene andesite under conditions of 1.0–2.0 GPa and 673–1073 K

enthalpy (0.35–0.42 eV) and the activation volume (−6.75 ± 1.67 cm^3/mole) measured here are lower than those obtained by Tyburczy and Waff (1983) at 0.78–1.17 eV and 3.25–17.9 cm^3/mole, respectively. And the values are also lower than those obtained by Laumonier et al. (2015) at 0.69–1.0 eV and 3.9–24.7 cm^3/mole, respectively. Discrepancies of temperature, melting conditions, the chemical composition and water content of samples are the important influential factors result in the difference between our results and previous studies.

Table 2

Fitted parameters for the electrical conductivity of pyroxene andesite

P (GPa)		T (K)	Log σ_0 (S/m)	ΔH (eV)	γ^2	ΔU (eV)	ΔV (cm^3/mol)
1.0	Heating	673–873	1.71	0.73	0.9949	–	–
1.0	Heating	923–1073	15.11	3.27	0.9913	–	–
1.0	Cooling	673–1073	1.00	0.42	0.9962	0.48 ± 0.04	−6.75 ± 1.67
1.5	Cooling	673–1073	1.31	0.37	0.9950		
2.0	Cooling	673–1073	1.05	0.35	0.9928		
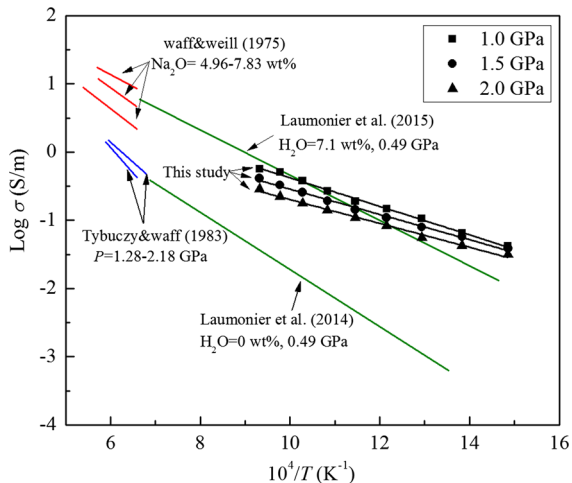
Figure 8
Comparisons of electrical conductivity of pyroxene andesite with previous studies

Figure 9
The photomicrograph of sample after experiment under conditions of 1.0 GPa and 873 K. Abbreviations in the figure represent *Px* pyroxene, *Qtz* quartz, *Pl* plagioclase and *Mt* magnetite

Dehydration, the most important process of water-bearing rocks, has a profound effect on the electrical conductivity and the activation enthalpy. In the present work, the electrical conductivity of pyroxene andesite increases rapidly when temperature rise beyond 873 K, at which point the activation enthalpy increases accordingly. Previous studies obtained the similar dehydration temperature with dacitic melts and amphibole-bearing rocks (Schmidbauer et al. 2000; Popp et al. 2006; Wang et al. 2012; Laumonier et al. 2015). Several other researchers have also proven that changes in the electrical conductivity and the activation enthalpy come from dehydration of hydrous rocks (Song et al. 1996; Zhu et al. 1999, 2001; Dai et al. 2014). Dehydration in pyroxene andesite begins at 873 K, as shown here and in previous studies (Schmidbauer et al. 2000; Wang et al. 2012), and the photomicrograph after experiment is shown in Fig. 9. Compared with the sample
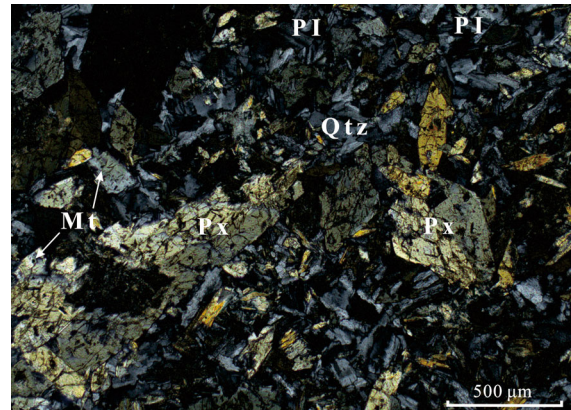
before experiment, the amphibole disappeared in the sample after experiment indicates that the dehydration reaction is sufficient. The new mineral phases are pyroxene, quartz and a few of magnetite ($\sim$1 %). It is worth noting that the magnetite is associated with pyroxene and quartz. These pyroxene and quartz should be considered to be the experimental products. By conducting a dehydration experiment on crocidolite in an oxidizing atmosphere, Addison and Sharp (1962) consider that the quality of crocidolite decreases after dehydration, and that free water is generated throughout the process. The reaction equation can be described as follow:

$$4Fe^{2+} + 4OH^- + O_2 \rightarrow 2H_2O + 4O^{2-} + 4Fe^{3+}$$

(4)
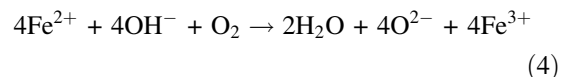
Amphibole, the main hydrous mineral in pyroxene, plays a crucial role in the rock's dehydration. By virtue of dehydration experiment on amphibole in a neutral atmosphere under different oxygen fugacity ($f_{O2} = 10^{-3}$–10^{-22} bar), Ernst and Wai (1970)

indicate that no free water is produced during amphibole dehydration. Instead, this process generates hydrogen. The reaction equation can be described as follows:

$$Fe^{2+} + OH^- \rightarrow \frac{1}{2}H_2 + O^{2-} + Fe^{3+} \qquad (5)$$
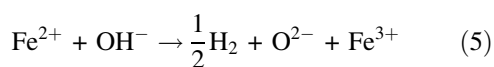
In this study, nickel foil and nickel disks controlled the test system's oxygen fugacity to a certain range. Oxygen fugacity under varying temperature and pressure can be calculated as follows:

$$Log\ (f_{O2})_{P,T} = A/T + B + C(P-1)/T \qquad (6)$$

where A and B are constants, T is the absolute temperature (K, <2273 K), P is the pressure (bar), $C = -\Delta V_s/2.303Q$, where ΔV_s stands for the bulk variation in mol volume of solid components before and after experimental reaction (cm^3/mol) and Q is the gas state constant [(cm^3 Pa)/(mol K)].

According to Li et al. (1998, 1999), A, B and C are -24930, 9.36 and 0.046 in solid oxygen buffer [NNO (Ni + NiO)]. The value of oxygen fugacity for pyroxene andesite is close to 10^{-18} bar at 1.0–2.0 GPa and 873 K, which falls within the same interval as the results obtained by Ernst and Wai (1970). Therefore, the reaction equation for pyroxene andesite, Eq. (5), is valid.

On the other hand, similar values obtained for the activation enthalpy before and after dehydration indicate that there is no variation in the conduction mechanism. The activation enthalpy has been investigated at length (Xu et al. 1998; Scarlato et al. 2004; Wu et al. 2010; Hui et al. 2015), as it is one of the most effective ways to define the conduction mechanism. Xu et al. (1998) reported that the activation enthalpy of perovskite is 0.61–0.70 eV at pressure of 25 GPa. Combining with the chemical composition of perovskite, Xu consider that the conduction mechanism for perovskite is the small polaron. Scarlato et al. (2004) calculated the activation enthalpy for different chemical compositions of basaltic melt from 0.35 to 0.82 eV at pressure of 0.9–1.5 GPa, and also identified that the small polaron is basaltic melt's conduction mechanism. Recently, Wu et al. (2010) indicated that the conduction mechanism for periclase is also the small polaron at temperature below 700 K. Hui et al. (2015) suggested that the activation enthalpy for quartz

andesite is 0.87–0.92 eV at pressure of 0.5–2.0 GPa, and the conduction mechanism for the grain interior conductivity of quartz andesite is the small polaron. The activation enthalpy of pyroxene andesite, as measured in this study, is in the same interval as previous studies. Furthermore, Tolland (1973) indicated that the electrical conductivity of Mg-rich amphibole is 0.57 eV along [010] and 0.54 along [001], respectively, and the conduction mechanism is the small polaron. Schmidbauer et al. (2000) also suggested that the charge transport mechanisms for Fe-bearing calcic amphiboles with different Fe concentrations are electron hopping between Fe^{2+} and Fe^{3+}. Based on these results on amphibole, the conduction mechanism for pyroxene andesite is more likely small polaron, not proton conduction, and the influence of water content is not considered here.

The activation volume is another important parameter to estimate the conduction mechanism. Shankland et al. (1993) calculated the activation volume of perovskite under different pressures as -0.26 cm^3/mol. Katsura et al. (2007) obtained the activation volume of ilmenite and perovskite under conditions of 25–35 GPa and 500–1200 K as -1.5 and -0.4 cm^3/mol, respectively. Dai et al. (2012) calculated the activation volume of different chemical composition of garnet as -1.4 ± 0.15 cm^3/mol. The activation volume of pyroxene andesite, as measured here (-6.75 ± 1.67 cm^3/mol), is in the same interval as previous studies.

The results of this study show that the electrical conductivity of pyroxene andesite decreases with increasing pressure. Nemours researches on olivine, garnet, and pyroxene have suggested that the electrical conductivity decreasing with increasing pressure represents the small polaron conduction (Xu et al. 2000; Yang et al. 2012; Dai and Karato 2014b). Hence, the activation enthalpies, the activation volume, together with relationship of electrical conductivity with pressure observed in this study indicate that the small polaron is the main conduction mechanism in pyroxene andesite.

In the end, the electrical conductivity of pyroxene andesite increases nearly 3 orders of magnitude after dehydration. Clowe et al. (1988) measured the ratio of ferric and total iron content after dehydration of different chemical composition of amphibole under different oxygen fugacity, and consider that the ratio

of Fe^{3+} and ΣFe increases 2–5 times after dehydration. Popp and Bryndzia (1992) measured the ferrous and ferric ion contents of amphibole, and found that 60 % of the ratio of $Fe^{3+}/\Sigma Fe$ is in the range of 0.2–0.5, and 35 % of the ratio is in the 0.5–1.0 range. Hirsch et al. (1993) measured the electrical conductivity of olivine with different iron contents and identified that a clear relationship between electrical conductivity and iron content; the electrical conductivity of olivine increases 1.39 times when iron content increases 20 %. Romano et al. (2006) investigated the electrical conductivity of garnet with different Fe and Al contents. Experimental data shows that the electrical conductivity of garnet increases with increasing almandine content. Notably, the electrical conductivity of almandine is 2.5 orders of magnitude higher than that of pyrope. Several prior researchers have indicated that increased carrier concentration is the most primary reason cause the increase of electrical conductivity of pyroxene andesite. However, it is possible that the observed high activation energy may somehow be related to the dehydration reaction and the conduction mechanism which requires further research.

5. Conclusions

The electrical conductivity of pyroxene andesite was measured under pressures of 1.0–2.0 GPa, temperatures of 673–1073 K, and 10^{-1}–4×10^6 Hz frequencies. Experimental data indicate that close relationships between the electrical conductivity of pyroxene and pressure, temperature, and frequency. The electrical conductivity of sample decreases with increasing pressure, while the activation enthalpy decreases accordingly. The activation energy and the activation volume are, respectively, 0.48 ± 0.04 eV and -6.75 ± 1.67 cm^3/mole after dehydration. The electrical conductivity of sample and the activation enthalpy increase rapidly while temperature reaches 873 K. Similarity in the activation enthalpy before and after dehydration indicates that there is no variation in the conduction mechanism. Combining with the chemical composition of pyroxene andesite, we consider that the conduction mechanism is the small polaron and that varying in carrier concentration results in increase of the electrical conductivity of sample.

REFERENCES

Addison, W. & E., Sharp, J. H. (1962). 716. Amphiboles. Part III. The reduction of crocidolite. *Journal of the Chemical Society (Resumed)*, 3693–3698.

Christensen, N. I., & Mooney, W. D. (1995). Seismic velocity structure and composition of the continental crust: a global view. *Journal of Geophysical Research, 100*(B6), 9761–9788.

Clowe, C. A., Popp, R. K., & Fritz, S. J. (1988). Exprimental investigation of the effect of oxygen fugacity on ferric-ferrous ratios and unit-cell parameters of four natural clinoamphiboles. *American Mineralogist, 73*, 487–499.

Dai, L. D., Hu, H. Y., Li, H. P., et al. (2014). Influence of temperature, pressure, and chemical composition on the electrical conductivity of granite. *American Mineralogist, 99*(7), 1420–1428.

Dai, L. D., Hu, H. Y., Li, H. P., et al. (2016). Influence of temperature, pressure, and oxygen fugacity on the electrical conductivity of dry eclogite, and geophysical implications. *Geochemistry, Geophysics, Geosystems, 17*, 2394–2407.

Dai, L. D., Jiang, J. J., Li, H. P., et al. (2015). Electrical conductivity of hydrous natural basalts at high temperatures and pressures. *Journal of Applied Geophysics, 112*, 290–297.

Dai, L. D., & Karato, S. (2009). Electrical conductivity of wadsleyite at high temperatures and high pressures. *Earth and Planetary Science Letters, 287*, 277–283.

Dai, L. D., & Karato, S. (2014a). High and highly anisotropic electrical conductivity of the asthenosphere due to hydrogen diffusion in olivine. *Earth and Planetary Science Letters, 408*, 79–86.

Dai, L. D., & Karato, S. (2014b). Influence of FeO and H on the electrical conductivity of olivine. *Physics of the Earth and Planetary Interiors, 237*, 73–79.

Dai, L. D., Li, H. P., Hu, H. Y., et al. (2012). The effect of chemical composition and oxygen fugacity on the electrical conductivity of dry and hydrous garnet at high temperatures and pressures. *Contributions to Mineralogy and Petrology, 163*(4), 689–700.

Dai, L. D., Li, H. P., Hu, H. Y., et al. (2013). Electrical conductivity of $Alm_{82}Py_{15}Grs_3$ almandine-rich garnet determined by impedance spectroscopy at high temperatures and high pressures. *Tectonophysics, 608*, 1086–1093.

Ernst, W. G., & Wai, C. M. (1970). Mössbauer, infrared X-ray and optical study of cation ordering and dehydrogenation in natural and heat treated sodic amphiboles. *American Mineralogist, 55*, 1226–1258.

Ferri, F., Gibert, B., Violay, et al. (2013). Electrical conductivity in a partially molten crust from measurements on metasedimentary enclaves. *Tectonophysics, 586,* 84–94.

Hirsch, L. M., Shankland, T. J., & Duba, A. G. (1993). Electrical conduction and polaron mobility in Fe-bearing olivine. *Geophysical Journal International, 114*(1), 36–44.

Hu, H. Y., Dai, L. D., Li, H. P., et al. (2015). Temperature and pressure dependence of electrical conductivity in synthetic anorthite. *Solid State Ionics, 276,* 136–141.

Huang, X. G., Bai, W. M., Xu, Y. S., et al. (2005a). Influence of hydrogen on electrical conductivity of wadsleyite and ringwoodite with its geodynamics implications. *Acta Petrological Sinica., 21*(6), 1743–1748. **(in Chinese with English abstract)**.

Huang, X. G., Huang, X. G., & Bai, W. M. (2012). Study on the electrical conductivity of carbonated peridotite. *Chinese Journal of Geophysics, 55*(9), 3144–3151. **(in Chinese with English abstract)**.

Huang, X. G., Xu, Y. S., & Karato, S. (2005b). Water content in the transition zone from electrical conductivity of wadsleyite and ringwoodite. *Nature, 434,* 746–749.

Huebner, J. S., & Dillenburg, R. G. (1995). Impedance spectra of hot, dry silicate minerals and rock-qualitative interpretation of spectra. *American Mineralogist, 80*(1–2), 46–64.

Hui, K. S., Zhang, H., Li, H. P., et al. (2015). Experimental study on the electrical conductivity of quartz andesite at high temperature and high pressure: evidence of grain boundary transport. *Solid Earth, 6,* 1037–1043.

Katsura, T., Yokoshi, S., Kawabe, K., et al. (2007). Pressure dependence of electrical conductivity of $(Mg, Fe)SiO_3$ ilmenite. *Physical Chemical Minerals, 34*(4), 249–355.

Laumonier, M., Gaillard, F., & Sifre, D. (2015). The effect of pressure and water concentration on the electrical conductivity of dacitic melts: implication for magnetotelluric imaging in subduction areas. *Chemical Geology, 418,* 66–76.

Li, H. P., Xie, H. S., Guo, J., et al. (1998). In situ control oxygen fugacity at high temperature and high pressure: a Ni-O system. *Geophysical Research Letters, 25*(6), 817–820.

Li, H. P., Xie, H. S., Guo, J., et al. (1999). In situ control oxygen fugacity at high temperature and high pressure. *Journal of Geophysical Research, 104*(B12), 29439–29451.

Nover, G. (2005). Electrical properties of crustal and mantle rocks—a review of laboratory measurements and their explanation. *Surveys In Geophysics, 26,* 593–651.

Nover, G., Will, G., & Waitz, R. (1992). Pressure-induced phase-transition in Mg_2GeO_4 as determined by frequency-dependent complex electrical-resistivity measurements. *Physics and Chemistry of Minerals, 19*(3), 133–139.

Popp, K. R., & Bryndzia, L. T. (1992). Statistical anaysis of Fe^{3+}, Ti, and OH in kaersutite from alkalic igneous rocks and mafic mantle xenoliths. *American Mineralogist, 77,* 1250–1257.

Popp, K. R., Hibbert, H. A., & Lamb, W. M. (2006). Oxy-amphibole equilibria in Ti-bearing calcic amphiboles: experimental investigation and petrologic implications for mantle-derived amphiboles. *American Mineralogist, 91*(1), 54–66.

Roberts, J. J., & Tyburczy, J. A. (1991). Frequency dependent electrical properties of polycrystalline olivine compacts. *Journal of Geophysical Research, 96*(B10), 16205–16222.

Romano, C., Poe, B. T., Kreidie, N., et al. (2006). Electrical conductivities of pyrope-almandine garnets up to 19 GPa and 1700 °C. *American Mineralogist, 91,* 1371–1377.

Scarlato, P., Poe, B. T., & Freda, C. (2004). High-pressure and high-temperature measurements of electrical conductivity in basaltic rocks from Mount Etna, Sicily, Italy. *Journal of Geophysical Research, 109*(B2), 210–220.

Schmidbauer, E., Kunzmann, T., Fehr, T., et al. (2000). Electrical resistivity and ^{57}Fe mössbauer spectra of Fe-bearing calcic amphiboles. *Physics and Chemistry of Minerals, 27*(5), 347–356.

Shankland, T. J., Peyronneau, J., & Poirier, J. P. (1993). Electrical conductivity of the earth's lower mantle. *Nature, 366,* 453–455.

Shinoda, K., Yamakata, M., Nanba, T., et al. (2002). High-pressure phase transition and behavior of protons in brucite $Mg(OH)_2$: a high-pressure–temperature study using IR synchrotron radiation. *Physics and Chemistry of Minerals, 29*(6), 396–402.

Song, M. S., Xie, H. S., Zheng, H. F., et al. (1996). Determination of serpentine dehydration temperature at 1–5 GPa by the method of electrical conductivity. *Chinese Science Bulletin, 41*(21), 1815–1819.

Tolland, H. G. (1973). Mantel conductivity and electrical properties of garnet, mica and amphibole. *Nature, 241,* 35–36.

Tyburczy, J. A., & Waff, H. S. (1983). Electrical conductivity of molten basalt and andesite to 25 kilobars pressure: geophysical significance and implications for charge transport and melt structure. *Journal of Geophysical Research, 88*(B3), 2413–2430.

Vanyan, L. L., & Gliko, A. O. (1999). Seismic and electromagnetic evidence of dehydration as a free water source in the reactivated crust. *Geophysical Journal International, 137*(1), 159–162.

Waff, H. S., & Weill, D. F. (1975). Electrical conductivity of magmatic liquids effects of temperature: effects of temperature, oxygen fugacity and composition. *Earth and Planetary Science Letters, 28*(2), 254–260.

Wang, D. J., Guo, Y. X., Yu, Y. J., et al. (2012). Electrical conductivity of amphibole-bearing rocks: influence of dehydration. *Contributions to Mineralogy and Petrology, 164,* 17–25.

Wu, X. P., Zhang, B. H., Xu, Y. S., et al. (2010). Electrical conductivity measurements of periclase under high pressure and high temperature. *Physica B, 405*(1), 53–56.

Xu, Y. S., McCammon, C., & Poe, B. T. (1998). The effect of alumina on the electrical conductivity of silicate perovskite. *Science, 282,* 922–924.

Xu, Y. S., Shankland, T. J., & Duba, A. G. (2000). Pressure effect on electrical conductivity of mantle olivine. *Physics of the Earth and Planetary Interiors, 118*(1–2), 149–161.

Yang, X. Z., Keppler, H., McCammon, C., et al. (2012). Electrical conductivity of orthopyroxene and plagioclase in the lower crust. *Contributions to Mineralogy and Petrology, 163*(1), 33–48.

Zhu, M. X., Xie, H. S., Guo, J., et al. (1999). Electrical conductivity measurement of serpentine at high temperature and pressure. *Chinese Science Bulletin, 44*(20), 1903–1907.

Zhu, M. X., Xie, H. S., Guo, J., et al. (2001). Impedance spectroscopy analysis on electrical properties of serpentine at high pressure and high temperature. *Science in China (Series D), 44*(4), 336–345.